Revision 2: The effect of H_2O on F and Cl solubility and solution mechanisms of in aluminosilicate melts at high pressure and high temperature.

Celia Dalou* and Bjorn O. Mysen

Carnegie Institution of Washington DC

5241 Broad Branch Rd, NW

Washington DC

now at:

Department of Geological Sciences,

The University of Texas at Austin,

Austin, Texas

ABSTRACT

Effects of H_2O on the solution behavior of fluorine and chlorine in peralkaline sodium aluminosilicate glasses quenched from melts at high temperature (1400˚C) and pressure (1.5 GPa) were studied by combining solubility measurements and Raman spectroscopy. With increasing H_2O content from 0 to ~ 10 wt%, the fluorine solubility increases from 3.3 to 4.4 mol% in Al-free glasses and from 6.3 to 9.3 mol% in Al-rich glasses (10 mol% Al_2O_3). In contrast, in the same H_2O concentration range the chlorine solubility decreases from 5.7 to 3.4 mol% in Al-free glasses and from 3.6 to 1.7 mol% in Al-rich glasses.

In Al-free glasses, interaction between H_2O and the silicate to depolymerize the network is $Q^4 + H_2O \leftrightarrow Q^2(H)$ and $Q^3 + H_2O \leftrightarrow Q^2(H)$. The effect of water on silicate

melt structure is different in halogen-bearing melts because in hydrous melt systems both F and Cl can act to depolymerize the melt further. For fluorine, this is accomplished via formation of Si-F, Al-F, and Na-F bonding in addition to Si-OH, whereas in chlorine-bearing hydrous melts, there is no interaction between Si^{4+} and Cl^{-}.

The halogen solubility in the magmatic liquid influences mineral/melt partition coefficients of chlorine and fluorine and implies partition coefficients different from unity. Moreover because of the contrasting effects of H_2O on fluorine and chlorine solubility, the Cl/F ratio in magmas formed in water-rich environments such as subduction zones can be a sensitive indicator H_2O during arc magmas genesis. Transport properties of melts, such as diffusion and viscosity, also vary differently in halogen-bearing hydrous melts compared with halogen-free systems. Moreover, the effects are the strongest in F-bearing systems.

keywords

Water, Fluorine, Chlorine, solubility, solution mechanism, aluminosilicate melt

INTRODUCTION

Fluorine and chlorine contents in phenocryst melt inclusions basaltic magma can reflect their respective compositions in the mantle source because the F and Cl contents of mantle-derived magma are less than their saturation values at low pressure. Therefore, unlike H_2O, F and Cl are not significantly degassed (e.g. Métrich and Wallace 2008). These halogens are also less affected by post-entrapment diffusive loss from melt

inclusions through the host mineral than other volatiles (e.g. Gaetani et al. 2012; Bucholz et al. 2013; Lloyd et al. 2013; Le Voyer et al. 2014), perhaps because of their low concentration in melt relative to their solubility in the melt. In the water-rich environment of island arc magma formation and evolution, the Cl/F- ratio of primitive island arc melt inclusions depends either on the composition of a metasomatic agent prior to melting of a source rock (Le Voyer et al. 2010) or on the fluid/rock ratio (Dalou et al. 2010), or both. Therefore, the Cl/F ratio may reflect the different fractionation of F and Cl during hydrous mantle melting depending on the proportion of H_2O (Dalou et al. 2010). This fractionation behavior with H_2O is either because of the effect of H_2O on melting phase relations and phase composition, by the effect of dissolved H_2O on the melt structure, or both.

In this paper, we focus on the role of melt structural changes with increasing H_2O content on the behavior of dissolved F and Cl. Fluorine and chlorine solubility and solution mechanisms in silicate melts previously have been studied in anhydrous aluminosilicate melt compositions (Mysen and Virgo 1985a, b; Kohn et al. 1991; Schaller et al. 1992; Zeng and Stebbins 2000; Stebbins and Du 2002; Mysen et al. 2004; Zimova and Webb 2006; Baasner et al. 2013; Dalou and Mysen 2012). In anhydrous melts, F and Cl solubility and solution mechanisms depend on Al content, Na/Si ratio and the proportion of network-modifier alkalis. In other words, solubility and solution mechanism in anhydrous melts depend on melt structure. Fluorine mainly forms complexes with Al in four or six-fold coordination and to a lesser extent Na-F complexes, depending on aluminosilicate melt composition (Mysen et al. 2004). In contrast, chlorine

bonds mainly with network-modifying cations such as alkali metals or alkaline earths (Stebbins and Du 2002; Sandland et al. 2004; Evans et al. 2008; Dalou and Mysen 2012).

Given the significant effect of H_2O on melt structure (e.g. Zhang et al. 1991; Schaller and Sebald 1995; Hess and Dingwell 1996; Zotov and Keppler 1998; Cody et al. 2005; Mysen and Cody 2005) and the halogen solubility is affected by melt structure, it is likely that H_2O plays an important role in F and Cl solution behavior in silicate melts. In this report, we have addressed effects of H_2O on F and Cl solubility and solution mechanisms in sodic aluminosilicate melts at 1.5 GPa and 1400ºC.

METHODS

Starting compositions were along the joins Na_2O-SiO_2-H_2O and Na_2O-Al_2O_3-SiO_2-H_2O, with H_2O content ranging from ~2 to 10 wt%. The nominal starting compositions are NS3Ax, NS4Ax and NS5Ax (x, representing the mol fraction of Al, while NS3 denotes $Na_2O•3SiO_2$; NS4 $Na_2O•4SiO_2$ and NS5 $Na_2O•5SiO_2$ in the Al-free glasses). Under the assumption that Al^{3+} is fully in tetrahedral coordination and is charge-balanced by Na^+, the degree of melt polymerization NBO/T is constant with the increasing of bulk melt Al/(Al + Si) ratio (Table 1).

Anhydrous starting glasses were prepared by mixing spectroscopically pure Na_2CO_3, SiO_2 and Al_2O_3. These mixtures were decarbonated during slow heating (50ºC /15 minutes) and then melted for 2 hours at ~ 100ºC above there liquidii (from 900 to 1400ºC, liquidus data from Osborn and Muan 1960). The melts were then quenched to glass, crushed for ~1h under alcohol and stored at ~250ºC when not in use. The powdered

93 starting glasses were loaded into 3mm outside diameter by 5-6 mm long Pt capsules,
94 together with double-distilled, deionized H_2O (from ~0.3 to ~1.6 µl depending on the
95 desired H_2O concentration), and with either $PdCl_2$ or AgF_2 as sources of chlorine and
96 fluorine, respectively. These latter two compounds break down to metal (Pd_0 or Ag_0) and
97 molecular Cl_2 or F_2, upon heating to experimental conditions (sufficient chloride and
98 fluoride was added to form ~ 5 wt% of Cl_2 or ~10 wt% of F_2 during high-temperature/-
99 pressure experiments). At experimental conditions, F and Cl are released from the
100 thermal decomposition of AgF_2 ($AgF_2 \rightarrow Ag_0 + F_2$) and $PdCl_2$ ($PdCl_2 \rightarrow Pd_0 + Cl_2$) with
101 metallic Ag and Pd forming spheres of metal (nm to 3 µm). Water was loaded in the
102 capsule first by using a 0.1 µl precision microsyringe. Then either $PdCl_2$ or AgF_2, and
103 finally the starting glasses were added before the capsule was welded shut. The maximum
104 of H_2O content used (~10 wt%) was less than that needed for water saturation of the melt
105 for their specific compositions, pressure and temperature conditions (Mysen and Cody
106 2005).

107 The samples, contained in those sealed Pt-capsules, were subjected to high
108 pressure (1.5 GPa) and high temperature (1400ºC) with 90-minute experimental duration
109 in 0.75" -diameter furnace assemblies (Kushiro 1976) in a solid-media, high-pressure
110 apparatus (Boyd and England 1960). Temperature was measured with $Pt/Pt_{90}Rh_{10}$
111 thermocouples to within ± 5ºC of the set point. From pressure-calibration with the quartz-
112 coesite transition (Bohlen 1984), the uncertainty is ±0.1 GPa. Before decompression,
113 experiments were quenched rapidly (±100ºC/s), by turning off the power to the furnace.

114 After experiments, capsules were opened and pieces of the glasses were either
115 kept intact to be examined by Raman spectroscopy or mounted in epoxy and polished for

SEM analysis. The rest of a sample was finely powdered under alcohol and dried to be used to determine H_2O content in a ThermoQuest Finnigan Delta^{plus}XL mass spectrometer. For these analyses, standards were stearic acid, mineral oil and pump oil. Prior to chemical analysis, the powdered samples (1-2 mg contained in Ag foil) were then stored for 12h at 50ºC under dry N_2 to reduce or eliminate, as much as possible, moisture from ambient air. A standard deviation of ~1.08 wt% of H_2O was obtained for the first session of IR-MS analysis and 1.21 wt% for the second.

Saturation of F and Cl was indicated by the presence of 10-30 μm bubbles in the quenched glass. Vapor exsolution upon quenching often produces finely distributed, micron- to submicron bubbles, significantly different from bubbles formed by stable vapor, which appeared as large bubbles (>10 μm) randomly distributed in the quenched glass (Mysen and Acton 1999). The absence of such bubbles in the sample (typically < 1 μm diameter) indicates that volatiles (water or halogens) did not exsolve from the glass during quenching.

Major elements, F, and Cl were analyzed energy dispersive mode with a JEOL JSM-6500F field emission scanning electron microscope SEM/EDS operating at 15 kV with a 0.1 nA beam current. To reduce Na losses during analysis, the beam was defocused of 25-50 μm. Possible Na, F or Cl loss were monitored by carrying out several analyses in the same sample spot. No significant compositional change (within the standard deviation) when using a 25 μm-diameter electron beam. At least 12 spots per glass were analyzed. Topaz was employed as standard for F and scapolite for Cl. Counting times used were 50 sec per element. Major element compositions of starting glasses are presented Table 1. The compositional homogeneity of the quenched glasses

suggests that 90 min experiment duration was sufficient to reach F and Cl equilibrium solubility in melts (Table 2, Figure 1).

The structure of the glasses including the structural environment of F and Cl was probed by using Raman spectroscopy. The Raman spectra were recorded with a JASCO model IRS-3100 confocal microRaman spectrometer with the 532 nm line of a solid-state laser operating at 6.4 mW at the sample for sample excitation. A 50X objective lens was employed for visual microscopic examination and spectroscopic analysis. Signal detection is provided by an Andor Model DV401-F1 1024*128 pixel (25 μm pixel size) Peltier-cooled CCD. With the 1200 grooves/mm of the holographic gratings, a 265–2110 cm^{-1} frequency range was covered within a single CCD window. The frequency resolution is ± 3 cm^{-1}. Acquisition time was typically 15 min per spectrum.

The background of Raman spectra was subtracted by applying a spline function through the portions of the spectra with no Raman intensity (Figure 2). After background correction, Raman spectra in the frequency region 800 to 1300 cm^{-1} (shaded range on Figure 2) were fitted to 5 to 6 Gaussian lines using the IGOR™ software package from Wavemetrics. Then number of fitted bands, their initial location and width were first chosen according to Mysen (2007). During the first step of the curve fitting process, the bandwidth was fixed. Then, the location and bandwidth were restricted to vary within 30 cm^{-1} until minimization of the χ^2. Finally, location, bandwidth, and band intensity, were used as free independent variables. Errors on the curve-fitting process are estimated from residuals, i.e. differences between the fitted model and the data, and are presented as estimated standard deviation of fitted location and intensity.

RESULTS AND DISCUSSION

1. Fluorine and chlorine solubility in quenched hydrous aluminosilicate melts (glasses)

The fluorine solubility is positively correlated with bulk H_2O content (Figure 1A). It increases linearly from 3.33 (±0.74) to 4.41 (±0.03) mol% in NS5 composition melt (no Al^{3+}) as the H_2O concentration increases from 0 to 9 wt%. In Al-bearing glass such as NS5A5 the F solubility increase is from 4.29 (±0.36) to 6.14 (±0.40) mol% in as the H_2O content is increased from 0 to 8.8 wt%, and from 6.32 (±0.37) to 9.31 (±0.31) mol% in NS5A10 when H_2O content increases from 0 to 10.7 wt%. In other words, the fluorine solubility is more sensitive to H_2O concentration in Al-bearing (NS5A10) than in Al-free melts (NS5). The solubility increases with bulk Al/(Al + Si) ratio at constant H_2O concentration.

There is a negative correlation of Cl solubility with H_2O concentration (Figure 1B), which contrasts with the fluorine solubility behavior (Figure 1A). The solubility decreases nearly linearly from 5.70 (±0.65) to 3.4 (±0.06) mol% in NS3 composition melt as the H_2O concentration is increased from 0 to 9 wt%, from 3.94 (±0.66) to 2.64 (±0.07) mol% in NS3A5 from 0 to 4.9 wt% H_2O, and from 3.62 (±0.38) to 1.66 (±0.04) mol% in NS3A10 in the H_2O from 0 to 8.5 wt%. The Cl solubility decreases, therefore, with the bulk Al/(Al + Si) in contrast with the solubility behavior of fluorine (Figures 1A and B). Moreover, the dependence of Cl solubility on H_2O content is greater in Al-free glasses than in Al-rich glasses (Cl/H_2O ratio is -0.25 in the NS3 system and -0.15 in the NS3A10

system). Negative relationships between Cl solubility and H_2O concentration in melt were also reported by Webster (1997) in haplogranite liquids. Although in the latter study the relationship between Cl solubility and H_2O content was distinctly non-linear. This difference could be because of the more complex composition of the haplogranitic liquids and because Webster (1997) conducted his experiments in a significantly lower pressure environment than in the present study.

2. F and Cl solution mechanisms in hydrous aluminosilicate glasses

2.1 Raman spectroscopic data and band assignments

Raman spectra in the frequency range of first order Raman scattering assigned to (Si, Al)-O stretch vibrations are presented in Figure 3 (between 800 and 1300 cm^{-1}; see, for example Mysen and Richet 2005, chapters 7 and 9 for review of data). There is a maximum between 1000 and 1100 cm^{-1} with visible shoulders on both sides, the detailed geometry of which is changing with H_2O and Al content (Figure 3).

Raman spectra of hydrous glasses were fitted to 5 bands, common both to F and Cl- bearing system, near 870-900, 930-970, 1010-1050, 1070-1110 and 1100-1150 cm^{-1}. These bands are also common in spectra of halogen-free, hydrous silicate and aluminosilicate glasses. Because of the compositional similarities (hydrous NS4Ax compositions), we used Mysen (2007) to assign the bands 870-900, 930-970, 1070-1110 and 1100-1150 cm^{-1} to (Si-Al)-vibrations in structural units with 3, 2, 1 and 0 non-bridging atoms for Q^1, Q^2, Q^3 and Q^4 structural units, respectively. The 870-900 cm^{-1}

band (light grey shading, Figure 4) is assigned to (Si,Al)-O^- (O^--nonbridging oxygen) vibrations in Q^1 structural units. Its area increases with the increasing H_2O content. The 930-970 cm^{-1} band (medium grey shading, Figure 4) is assigned to (Si,Al)-O^- in Q^2 units, the 1070-1110 cm^{-1} (dark grey shading) to (Si,Al)-O^- vibrations in Q^3, and the 1100-1150 cm^{-1} band (carbon black shading) to (Si,Al)-O^o (O^o-bridging oxygen) in Q^4 units. This assignment is consistent with the structural interpretation of recent ^{29}Si NMR spectra of glasses along the join $Na_2Si_3O_7$-$Na_2(NaAl)_3O_7$ (Mysen et al. 2003) and in the system Na_2O-SiO_2-H_2O (Cody et al. 2005).

The assignment of the peak near 1010-1050 cm^{-1} has been proposed to be either to Si-O^o or (Si,Al)-O^o vibrations in any structural unit with bridging oxygen (Mysen et al. 1982; Lasaga 1982) or to Si-O vibrations of bonds associated with alkali metals or alkaline earths in Q^3 species (Fukumi et al. 1990; McMillan et al. 1992). However, no evidence of a second Q^3 structural unit was found in the ^{29}Si NMR spectra in aluminosilicate glasses of compositions similar to the ones used in this study (e.g. Maekawa et al. 1991; Buckermann et al. 1992; Mysen et al. 2003; Cody et al. 2005). Therefore, the most likely assignment is the (Si,Al)-O° vibration.

The curve fitting of the spectra of F-bearing glasses requires an additional band (Table 5) around 980-990 cm^{-1} (crossed-hatched region in Figure 4). The fits to spectra of Cl-bearing equivalent glasses or halogen-free glasses of similar composition either anhydrous or hydrous glasses do no require this additional band (Mysen 2007). A band near ~945 cm^{-1} has been assigned to correspond to SiO_3-F complexes (Dumas et al. 1982; Yamamoto et al. 1983). As the F/O increases, the frequency of the band assigned to SiO_xF_{4-x} complexes increases (Yamamoto et al. 1983; Mysen and Virgo 1985a, 1985b).

Accordingly, the 990 cm^{-1} band is assigned to (Si, Al)-F stretching in Q^3, in which one or two non-bridging oxygens are replaced by F.

With increasing H_2O content and Al/(Al+Si) ratio of glasses, peak positions shift to the lower frequencies, more particularly for the band attributed Q^4 (Table 3). An analogous shift has been observed in ^{29}Si NMR MAS NMR spectra (e.g. Zotov and Keppler 1998; Lee and Stebbins 1999). The shift is mainly observed Q^4 bands, because Al^{3+} preferentially substitutes for Si^{4+} in the most polymerized Q^n species (Merzbacher and White 1991; Mysen et al. 2003). The decrease of Q^4 peak frequency with increasing H_2O content (Table 3), previously also reported by Zotov and Keppler (1998), may reflect the preference of OH to bond with Si in Q^4, rather than with Al, increasing the proportion of Al in Q^4.

2.2 Structural interpretations

In order to quantify and decipher the effect of H_2O, F, and Cl on melt structure, relative band intensities must be converted in Q^n-species mol fraction abundances. Mol fraction of structural units, X_{Q1}, X_{Q2}, X_{Q3} and X_{Q4}, were calculated by using Raman literature data (Mysen and Frantz 1993; Mysen and Cody 2001; Mysen et al. 2003; Mysen et al. 2004) and ^{29}Si-NMR spectral data of glasses of similar composition. This calculation derives mol fraction X_n, for species, n, from ^{29}Si MAS NMR, combining a calibration factor α_n with integrated intensity of the relevant Raman band, A_n, (Cody et al. 2005; Mysen and Cody 2005):

$$\alpha_n = X_n / A_n. \quad (1)$$

The α_n-factors for Q^1, Q^2 and Q^3 based on NMR and Raman data are from hydrous NS4 and NS4A10 glasses of Cody et al. (2005) and Mysen and Cody (2005). The Al/(Al + Si) has no effect on all α_n-factors, except for α_4 (Mysen 2007). The H_2O content in glasses has only a small effect. Nevertheless, by using α_n-factors determined from halogen-free glasses, we may have introduced an inaccuracy in the calculation Q^n mol fractions in halogen-bearing glasses. The extent of this uncertainty is not readily estimated.

Essentially all the Al^{3+} resided in the Q^4 species in peralkaline aluminosilicate melts and glasses (Merzbacher and White 1991; Mysen et al. 2003), which is why the α_4 depends on Al/(Al+Si) in the Q^4- species. The Al/(Al + Si) of the present glasses cannot be calculated and likely varies with H_2O and halogen content. The Q^4-abundance hydrous aluminosilicate glasses was calculated, therefore, from mass-balance:

$$X_{Q4} = 1 - (X_{Q3} + X_{Q2} + X_{Q1}). \quad (2)$$

The uncertainty of this procedure is related to the unknown amount of $Si(Q^3)$-OH, $Si(Q^3)$-F and $Si(Q^3)$-Cl, which are not taken into account in this calculation.

The variation of Q^n species abundance with H_2O content in Al-free (Figure 5) and Al-rich samples (Figure 6) is different in the halogen-free samples from Mysen (2007) and the F- or Cl-bearing samples examined here.

2.2.1 The structural effect of H_2O on silicate glasses

Structural characterization of hydrous, halogen-bearing glasses relies on existing structural data of hydrous, halogen-free aluminosilicate glasses (Mysen 2007). In such

hydrous glasses, increasing H_2O content produces a linear increase of X_{Q1}. However, the X_{Q2} abundance increase is non-linear. This solution mechanism can be illustrated with the expression;

$$Q^4 + H_2O = Q^2(2H), \quad (3)$$

where $Q^2(2H)$ refers to Q^2-species with $2H^+$ per Si, which is consistent with the data from the present study (Figure 5).

The X_{Q3} abundance initially also increases non-linearly followed by a decrease for high H_2O content. At low H_2O content (< 4 wt%), the Q^3 abundance increases with increasing water concentration, because Na^+ preferentially forms bonding with nonbridging oxygens in Q^3-species with the H^+ associated with nonbridging oxygen in Q^2 and Q^1 species (Mysen 2007). Above 4 wt% H_2O (~ 9 mol% H_2O), the decreasing Q^3 abundance likely is due to additional breaking of oxygen bridges to form more $Q^2(2H)$ are in Q^3 species:

$$Q^3 + 2H_2O = Q^2(2H). \quad (4)$$

For these compositions, the X_{Q4} abundance always decreases with increasing water content (Mysen 2007).

In melts with high sodium contents, solution of water does not significantly increase depolymerization (Cody et al. 2005). Therefore, the assumption that H^+ forms complexes only with silica to create non-bridging oxygens cannot be correct. The presence of Na-OH was suggested by ^1H SPMAS NMR studies of NS4 composition hydrous glasses (Xue and Kanzaki 2003; Cody et al. 2005). The formation of such complexes causes polymerization of the silicate network (Mysen and Cody 2005), because it decreases the abundance of Na^+ network modifiers. As Na/Si increases, the

300 formation of Na-OH complexes increases (Cody et al. 2005; Mysen and Cody 2005).

301 The structure of hydrous halogen-bearing glasses of the present study is compared
302 with hydrous halogen-free glasses from Mysen (2007). It must be noted that the NBO/T
303 of Mysen (2007)'s glasses is slightly lower than ours (0.44) and the H_2O content in the
304 two studies was carried out by different methods. Nevertheless, NBO/T-difference
305 between the two studies is nearly within their error bars, so it is assumed that Q^n trends
306 with increasing H_2O content can be compared (Figure 7).

307 **In hydrous F-bearing melt glasses**, X_{Q2} and X_{Q4} are lower and X_{Q3} is higher
308 than in halogen-free systems. Moreover, the X_{Q2} increase and X_{Q4} decrease with
309 increasing H_2O content are lower in F-bearing glasses than in F-free glasses. These latter
310 observations suggest that the presence of F affects depolymerization reactions such as,
311 for example, described in equation 3.

312 In Na_2O-SiO_2-F glasses, the dominant complexes, inferred from ^{19}F and ^{29}Si
313 NMR spectroscopy, have been reported as NaF type (e.g. Schaller et al. 1992; Mysen et
314 al. 2004). The Si-F complexes were found by Raman spectroscopy studies in high F
315 concentration SiO_2-NaF glasses (> 7.5 mol% of F; Mysen and Virgo 1985b). In addition,
316 a small fraction of Si-F bonding was found by ^{19}F NMR spectroscopy in F-bearing
317 silicate and aluminosilicate glasses (Zeng and Stebbins 2000; Kiczenski et al. 2004;
318 Kiczenski and Stebbins 2006). Mysen and Virgo (1985b) show that the proportion of Na-
319 F and Si-F complexes depends on the degree of polymerization of glasses: the abundance
320 of Na-F is greater than Si-F complexes in highly depolymerized Na_2O-SiO_2-F glasses
321 (NBO/T ~ 2), but in melt of comparable NBO/T to that in this study (~ 0.4, 0.5), Si-F
322 complexes represents 90% of fluoride complexes.

In hydrous fluorine-bearing melts, Si-F complexes most likely is in the form a Q^3-type complex where one of the oxygen per Si is replaced with fluorine to form a stoichiometry such as, $Si_2O_3F_2$. We will denote this as $Q^3(F)$. Water breaks oxygen bridges to form Si-OH bonds. Given that the Raman spectra indicate increased abundance of Q^2-species with increasing H_2O content, it is proposed that the stoichiometry of this species is SiO_3H_2. A schematic and balanced reaction to illustrate how fluorine interacts with the silicate network then becomes;

$$3Q^4 + H_2O + F_2 = 2Q^3(F) + Q^2(H) + 1/2O_2, \quad (5)$$

where Q^4 is equivalent to SiO_2, $2Q^3(F)=Si_2O_3F_2$, and $Q^2(H)=SiO_3H_2$.

One could also write equations with H^+ in species other than Q^2 and fluorine in species other than Q^3. However, from the Raman spectra, there is evidence only for formation of Q^3 and Q^2. Moreover, other evidence suggests that H^+ tends to favor associated with nonbridging oxygen in the least polymerized species. In the present study, that species is Q^2. The actual reaction likely is more complex and will need to accommodate Na^+ and Al^{3+} so that there will be mixed (Al,Si) species and mixed (Na,H) species. Finally, in a hydrous alkali aluminosilicate melt system such as examined here, fluorine bonding to Al^{3+} and Na^+ also is likely as demonstrated in other F-bearing anhydrous glasses (e.g., Schaller et al. 1992; Mysen et al. 2004). Although a number of feasible solution mechanisms involving those components could be written, there is little structural information with which to identify the most likely reaction, so this has not been attempted.

In hydrous Cl-bearing glasses, the abundance of Q^4, X_{Q4} is lower and X_{Q3} is higher than in halogen-free melts, which implies that Cl enhances melt depolymerization

(Figure 7). Raman and ^{35}Cl NMR spectroscopy (Stebbins and Du 2002; Sandland et al. 2004; Evans et al. 2008; Dalou and Mysen 2012) show that Cl^- form bonds with alkali network modifiers in silicate glass and melt. Sodium is the network-modifier in the present study. As H_2O content in Cl-bearing glasses increases, the Q^2 abundance increases and that of Q^4 decreases more rapidly than in Cl-free, hydrous glasses (Figure 5). In other words, Cl enhances H_2O depolymerizing effect. Given that there is no evidence for Si-Cl bonding and that Cl both likely form NaCl complexes and increase H_2O depolymerization effect, our data are consistent with the following reaction schematic expression:

$$Q^3(Na) + Q^4 + Cl_2 + 2H_2O = 2Q^2(H) + NaCl + 1/2O_2. \quad (6)$$

In eqn. (6), $Q^3(Na)$ is equivalent to $Na_2Si_2O_5$, where, in other words, the nonbridging oxygens are charge-balanced with Na^+, and $Q^2(H)=SiO_3H_2$, where the nonbridging oxygens are charge-balanced with 2 H^+. The Q^4 is equivalent to SiO_2. We emphasize that this is schematic as (Al,Si)-exchange is not taken into account.

Expression (6) also illustrates how stabilization of NaCl complexes in hydrous melts results in melt depolymerization, whereas in anhydrous melts, formation of similar NaCl complexes results in silicate polymerization via a simple expression such as, for example:

$$2Q^3(Na) + Cl_2 = 2Q^4 + 2NaCl + 1/2O_2. \quad (7)$$

2.2.2 The structural effect of Al/(Al+Si) proportion on hydrous silicate glasses

In order to understand the role of Al^+ in solution of halogens, a summary of how Al^{3+} interacts with melt structure is necessary. In this environment as well as in crystalline

aluminosilicates, charge-balanced Al^{3+} substitutes for Si^{4+} in the silicate species with the smallest intertetrahedral angle (Brown et al. 1969; Merzbacher and White 1991; Mysen et al. 2003). In peralkaline aluminosilicate melts with coexisting Q^4, Q^3, and Q^2 species, the substitution will be dominantly in the form of aluminous Q^4 units, or simply $NaAlO_2$.

Fluorine solution in anhydrous aluminosilicate melts results in formation of both Al-F and Na-F bonding (e.g. Schaller et al. 1992; Zeng and Stebbins 2000; Mysen et al. 2004; Baasner et al. 2014). The Al-F/Na-F ratio increases with increasing Al/(Al+Si) of the melt (Mysen et al. 2004). One may write such a mechanism by using the Q^3(F) complex discussed above [equation (5)] as source of fluorine and by describing dissolved Al^{3+} as an AlO_2 complex. The two principal reactions can be written:

$$2Q^3(F) + 2NaAlO_2 = 2Q^1(Al) + 2NaF \quad (8a)$$

and

$$3Q^3(F) + 2NaAlO_2 = 2Q^3(Na) + 2AlF_3 + 4Q^4. \quad (8b)$$

In these two expressions, the notations NaF and AlF_3 simply are meant to indicate stoichiometric environments with Na-F and Al-F bonding, respectively, and the notations Q^1(Al) and Q^3(Na) means nonbridging oxygen bonded to Al^{3+} and Na^+, respectively. The implications of eqns. (8a) and (8b), is that formation of Al-F bonding in an anhydrous peralkaline aluminosilicate melts, is a much more efficient way to depolymerize the melt than by forming Na-F bonds.

In hydrous aluminosilicate systems, the additional depolymerization reaction is illustrated in equation (4), which can be combined with equations (8a) and (8b) to indicate the two additional solution mechanisms [in addition to eqn. (5)] resulting from the presence of charge-balanced Al^{3+} in a hydrous melt:

392 $2Q^3(F) + Q^4 + H_2O + 2NaAlO_2 = 2Q^1(Al) + 2NaF + Q^2(H)$, (9a)

393 and

394 $3Q^3(F) + 2NaAlO_2 + H_2O = 2Q^3(Na) + 2AlF_3 + 3Q^4 + Q^2(H)$. (9b)

395 So even though addition of water to fluorine-bearing peralkaline aluminosilicate melts
396 results in additional silicate depolymerization, the difference on between Al-F and Na-F
397 discussed under eqns. (8a) and (8b) remains.

398 The solution mechanisms illustrated with expressions (5, 9a, and 9b) show the
399 principles. However, given that Si-F, Na-F, and Al-F bonding have been detected in F-
400 bearing aluminosilicate melts (Schaller et al. 1992; Zeng and Stebbins 2000; Mysen et al.
401 2004), very likely all three mechanisms work together with their relative importance
402 governed by the Al/(Al+Si) of the melts [as already seen in anhydrous F-bearing
403 aluminosilicate melts – see Mysen et al. (2004)]. The spectroscopic data in the present
404 report are insufficient detailed to establish those details.

405 **In hydrous Cl-bearing aluminosilicate glasses,** the Cl solution mechanism
406 remains unclear because we do not have an understanding of the type of Al-Cl-Na formed
407 in anhydrous aluminosilicate melts. Complexes that incorporate Na-Cl bonding most
408 commonly are reported (e.g. Stebbins and Du 2002; Sandland et al. 2004, Zimova and
409 Webb 2006; Evans et al. 2008; Baasner et al. 2013). In an anhydrous aluminosilicate
410 melt, such complexes may be formed via the solution mechanism;

411 $12Q^4 + 4NaAlO_2 + 2Cl_2 = 4NaCl + 6Q^3(Al) + O_2$, (10a)

412 whereas if Al-Cl bonding is formed (indicated by $AlCl_3$ in the schematic expressions):

413 $4Q^4 + 4NaAlO_2 + 6Cl_2 = 4AlCl_3 + 4Q^3(Na) + 3O_2$. (10b)

414

In equations (10a,b), as above, we consider Al^{3+} predominantly in Q^4 and denote it $NaAlO_2$. The symbolism $Q^3(Na)$ and $Q^3(Al)$ indicates, as above, Na^+ and Al^{3+} respectively as network-modifying cations forming bonding with nonbridging oxygen in Q^3-species. This means that $2Q^3(Na)$ is equivalent to $Na_2Si_2O_5$ and $6Q^3(Al)$ equivalent to $Al_2(Si_2O_5)_3$. This means that in anhydrous melts, formation of NaCl-type depolymerizes anhydrous aluminosilicate melts more efficiently than formation of Al-Cl bonding with $AlCl_3$-type complexes.

In the hydrous systems under considerations here, these relationships remain except that by dissolving H_2O in Cl-bearing aluminosilicate melts, additional depolymerization will take place with the protons forming OH-bonding by reacting with nonbridging oxygen in depolymerized units. As above, we consider this to be Q^2 units as discussed above. The complete, schematic solubility mechanisms of water and chlorine in aluminosilicate melts can be written:

$$14Q^4 + 4NaAlO_2 + H_2O + 2Cl_2 = 4NaCl + 6Q^3(Al) + Q^2(H) + O_2, \quad (11a)$$

and

$$5Q^4 + 4NaAlO_2 + H_2O + 6Cl_2 = 4AlCl_3 + 4Q^3(Na) + Q^2(H) + 3O_2. \quad (11b)$$

It is likely that in actuality, mechanisms (6, 11a,b) operate together and that the relative importance, depends not only on water and chlorine content, but also on Al/(Al+Si), and Na/(Al+Si).

IMPLICATIONS: Contrasting effects of H_2O on F and Cl complexes in alumino-silicate melts

438 An increase of both H_2O and the Al/Al+Si proportion leads to enhance fluorine
439 solubility in aluminosilicate melts such as natural magmatic melts. The effect of
440 dissolved H_2O on F solubility increases with the increasing Al/Al+Si because H_2O
441 suppresses the relative importance of Si-F complexing. The effect of Al/(Al+Si) is less
442 important for chlorine-bearing aluminosilicate melts because Si-Cl bond formation does
443 not seem to take place. The influence of water on silicate polymerization of chlorine-
444 bearing melts is, therefore, less important than that of fluorine.

445 Properties of hydrous, fluorine-bearing magma vary with water content, but the
446 magma composition affects the extent of the water effect. This may, for example help
447 explaining why diffusivity of fluorine in basaltic magma is more sensitive than in
448 phonolite (Alletti et al. 2007; Balcone-Boissard et al. 2009). Note that the type of alkali
449 present in melts has no significant influence of F properties, as solubility (Dalou et al. in
450 review) or diffusivity (Balcone-Boissard et al. 2009). In the latter melt composition, the
451 higher silica concentration enhances fluorine solution as Q^3(F) species compared with
452 solution to form Na-F or Al-F bonding, or both. Increasing water content in an Q^3(F)-rich
453 melt is less efficient silicate depolymerizer than when fluorine complexing is dominated
454 by Al-F and/or Na-F bonding, as likely is the case in hydrous basaltic magma. As
455 diffusivity is positively correlated with degree of polymerization of silicate melts, it
456 follows, then, that water has a more pronounced effect on F diffusion in basaltic than in
457 phonolitic melts.

458 Interestingly, the Cl diffusivity in hydrous phonolitic and basaltic magmas is more
459 sensitive to water content in the silica-rich phonolite melts (Alletti et al. 2007; Balcone-
460 Boissard et al. 2009). This behavior likely is related to the fact that ion contrast to

fluorine, chlorine does not form bonding with Si^{4+}. Relative variations in water effects on properties of Cl-bearing magmas are, therefore, simply a function of the proportion of alkali-fluorine versus aluminum-fluorine complexing. The alkali/(Al+_Si) of phonolite is considerably greater in phonolite than in basalt melt so that likely alkali-chloride complexing is more important. From equation (11), water affects melt polymerization more profoundly in environments where alkali-chloride complexing is the most important solution behavior. As a result, Cl-bearing phonolite melt is more sensitive to water than is basalt melt.

The increase of F solubility with increasing H_2O content is consistent with the decrease of mineral/melt partition coefficients of F with increasing H_2O content dissolved in basaltic melts (Dalou et al. 2010). Similarly, the Cl solubility decrease with increasing H_2O content is consistent with the decrease of Cl partition coefficients between anhydrous mantle minerals and hydrous basaltic melts, with increasing H_2O content dissolved in basaltic magmas (Dalou et al. 2010). Because of the contrasting effect of H_2O on F and Cl mineral/melt partition coefficients, Dalou (2011) highlight the potential of F and Cl as tracers of primary H_2O content in mantle magmas, especially in subduction zones' magmas. Indeed, the variation of a few wt% of H_2O produces highly variable Cl/F ratios in magmas. We suggest that halogen solubility in the magmatic liquid has a significant influence on F and Cl mineral/melt partition coefficients and because the effect of the dissolved water on F and Cl solubility differs, the Cl/F ratio in magmas is sensitive to the amount of H_2O involved in arc magmas genesis.

Aknowledgments: This research was conducted with partial support from NSF grant EAR-1212754 (to BOM and CD), and NAI grant to the Geophysical Laboratory. Reviews by Hélène Balcone-Boissard, two anonymous reviewers and A.E. Daniel Neuville were very helpful. We also thank J.T. Armstrong and K. Crispin for their help with the optimization of the SEM/EDS analytical protocol, and R. Bowden for her help in analyzing samples H_2O content on the mass spectrometer.

REFERENCES

Alletti, M., Baker, D.R., and Freda, C. (2007) Halogen diffusion in a basaltic melt. Geochimica et Cosmochimica Acta, 71(14), 3570-3580.

Baasner, A., Schmidt, B.C., and Webb, S.L. (2013) Compositional dependence of the rheology of halogen (F, Cl) bearing-aluminosilicate melts. Chemical Geology, 346(C), 172-183.

Baasner, A., Schmidt, B.C., Dupree, R., and Webb, S.L. (2014) Fluorine speciation as a function of composition in peralkaline and peraluminous Na_2O-CaO-Al_2O_3-SiO_2 glasses: A multinuclear NMR study. Geochimica et Cosmochimica Acta, 132, 151-169.

Balcone-Boissard, H., Baker, D.R., Villemant, B., and Boudon, G. (2009) F and Cl diffusion in phonolitic melts: Influence of the Na/K ratio. Chemical Geology, 263(1), 89-98.

Bohlen, S.R. (1984) Equilibria for precise pressure calibration and a frictionless furnace assembly for the piston-cylinder apparatus. Neues Jahrbuch für Mineralogie, Mh.,

84, 404–412.

Boyd, F.R. and England, J.L. (1960) Apparatus for phase equilibrium measurements at pressures up to 50 kilobars and temperatures up to 1750°C. Journal of Geophysical Research, 65, 741–748.

Brown, G. E., Gibbs, G. V., and Ribbe P. H. (1969) The nature and variation in length of the Si-O and Al-O bonds in framework silicates. American. Mineralogist, 54, 1044–1061.

Bucholz, C.E., Gaetani, G.A., Behn, M.D., Shimizu, N. (2013) Post-entrapment modification of volatiles and oxygen fugacity in olivine-hosted melt inclusions. Earth and Planetary Science Letters, 374, 145-155.

Buckermann, W. A., Müller-Warmuth, W., and Heinz Frischat, G. (1992) A further ^{29}Si MAS NMR study on binary alkali silicate glasses. Glastechnische Berichte, 65(1), 18-21.

Cody, G.D., Mysen, B.O., and Lee, S.K. (2005) Structure vs. composition: A solid-state ^{1}H and ^{29}Si NMR study of quenched glasses along the Na_2O-SiO_2-H_2O join. Geochimica et Cosmochimica Acta, 69(9), 2373–2384.

Dalou, C. (2011) Fluorine and chlorine fractionation in the sub-arc mantle: an experimental investigation. 304p. Ph.D. thesis, Université Blaise Pascal, Clermont-Ferrand. *http://tel.archives-ouvertes.fr/tel-00657297*

Dalou, C., and Mysen, B.O. (2012) Solubility and solution mechanisms of chlorine in aluminosilicate melts at high pressure and high temperature**.** *American Geophysical Union, Fall Meeting 2012, abstract #MR11C-2509.*

528 Dalou, C., Koga, K.T. and Shimizu, N. (2010) Fluorine and Chlorine behavior in mantle
529 wedge, new implications for slab component. *American Geophysical Union, Fall*
530 *Meeting 2010, abstract #V34C-06.*
531 Dalou, C., Mysen, B.O., and Cody, G.D. (*in review*) Solubility and solution mechanisms
532 of fluorine and chlorine in aluminosilicate melts at high pressure and high
533 temperature**.** American Mineralogist**.**
534 Dumas, P., Corset, J., Carvalho, W., Levy, Y., Neuman, Y. (1982) Fluorine-doped
535 vitreous silicate analysis of fiber optics preforms by vibrational spectroscopy.
536 Journal of Non-Crystalline Solids, 47, 239-242.
537 Evans, K.A., Mavrogenes, J.A., O'Neill, H.S., Keller, N.S., and Jang, L.Y. (2008) A
538 preliminary investigation of chlorine XANES in silicate glasses. Geochemistry,
539 Geophysics, Geosystems, 9(10).
540 Fukumi, K., Hayakawa, J., and Komiyama, T. (1990) Intensity of Raman band in silicate
541 glasses. Journal of Non-Crystalline Solids, 119(3), 297-302.
542 Gaetani, G.A., O'Leary, J.A., Shimizu, N., Bucholz, C.E., and Newville, M. (2012)
543 Rapid reequilibration of H_2O and oxygen fugacity in olivine-hosted melt
544 inclusions. Geology, 40(10), 915-918.
545 Hess K.-U., and Dingwell D. B. (1996) Viscosities of hydrous leucogranitic melts: A
546 non-Ahrrenian model. American Mineralogist, 81, 1297-1300.
547 Kiczenski, T.J., Du, L.S., and Stebbins, J.F. (2004) F-19 NMR study of the ordering of
548 high field strength cations at fluoride sites in silicate and aluminosilicate
549 glasses. Journal of non-crystalline solids, 337(2), 142-149.

Kiczenski, T.J., and Stebbins, J.F. (2006) The effect of fictive temperature on the structural environment of fluorine in silicate and aluminosilicate glasses. Journal of the American Ceramic Society, 89(1), 57-64.

Kohn, S.C., Dupree, R., Mortuza, M.G., and Henderson, C.M.B. (1991). NMR evidence for five- and six- coordinated aluminum fluoride complexes in F-bearing aluminosilicate glasses. American Mineralogist, 76, 309-312.

Kushiro, I. (1976) A new furnace assembly with a small temperature gradient in solid-media, high-pressure apparatus. Carnegie Institution Washington year Book, 75, 832-833.

Lasaga A.C. (1982) Optimization of CNDO for molecular orbital calculation on silicates. Physics and Chemistry of Minerals, 8, 36-46.

Lee, S.K., and Stebbins, J.F. (1999) The degree of aluminum avoidance in aluminosilicate glasses. American Mineralogist, 84(5-6), 937-945.

Lee, S.K., and Stebbins, J.F. (2009) Effects of the degree of polymerization on the structure of sodium silicate and aluminosilicate glasses and melts: An ^{17}O NMR study. Geochimica et Cosmochimica Acta, 73(4), 1109-1119.

Le Voyer, M., Rose-Koga, E.F., Shimizu, N., Grove, T.L., and Schiano, P. (2010) Two Contrasting H_2O-rich Components in Primary Melt Inclusions from Mount Shasta. Journal of Petrology, 51, 1571–1595.

Le Voyer, M., Asimow, P.D., Mosenfelder, J.M., Guan, Y., Wallace, P.J., Schiano, P., Stolper, E.M., and Eiler, J.M. (2014) NanoSIMS determination of H_2O and F concentrations in olivines around melt inclusions, Journal of Petrology, doi:10.1093/petrology/egu003.

Lloyd, A.S., Plank, T., Ruprecht, P., Hauri, E.H., and Rose, W. (2013) Volatile loss from melt inclusions in pyroclasts of differing sizes. Contributions to Mineralogy and Petrology, 165(1), 129-153.

Maekawa, H., Maekawa, T., Kawamura, K., and Yokokawa, T. (1991) The structural groups of alkali silicate glasses determined from ^{29}Si MAS-NMR. Journal of Non-Crystalline Solids, 127(1), 53-64.

Merzbacher, C.I., and White, W.B. (1991) The structure of alkaline earth aluminosilicate glasses as determined by vibrational spectroscopy. Journal of non-crystalline solids, 130(1), 18-34.

Métrich, N., and Wallace, P.J (2008) Volatile abundances in basaltic magmas and their degassing paths tracked by melt inclusions. Reviews in Mineralogy and Geochemistry, 69(1), 363-402.

McMillan, P.F., Wolf, G.H., and Poe, B.T. (1992) Vibrational spectroscopy of silicate liquids and glasses. Chemical Geology, 96(3), 351-366.

Mysen, B.O. (2007) The solution behavior of H_2O in peralkaline aluminosilicate melts at high pressure with implications for properties of hydrous melts. Geochimica et Cosmochimica Acta, 71(7), 1820-1834.

Mysen, B.O., and Virgo, D. (1985a) Structure and properties of fluorine-bearing aluminosilicate melts: the system Na_2O-AI_2O_3-SiO_2-F at 1 atm. Contributions to Mineralogy and Petrology, 91, 205–220.

Mysen, B.O., and Virgo, D. (1985b) Interaction between fluorine and silica in quenched Melts on the joins SiO_2-AIF_3 and SiO_2-NaF determined by Raman spectroscopy. Physics and chemistry of minerals, 12, 77-85.

596 Mysen, B.O., and Frantz, J.D. (1993) Structure of silicate melts at high temperature: In-
597 situ measurements in the system $BaO-SiO_2$ to 1669ºC. American Mineralogist, 78(7-
598 8), 699-709.
599 Mysen, B.O., and Acton, M. (1999) Water in H_2O-saturated magma-fluid systems:
600 solubility behavior in $K_2O-Al_2O_3-SiO_2-H_2O$ to 2.0 GPa and 1300°C. Geochimica et
601 Cosmochimica Acta, 63(22), 3799-3815.
602 Mysen, B.O., and Cody, G.D. (2001) Silicate-phosphate interactions in silicate glasses
603 and melts: II. Quantitative, high-temperature structure of P-bearing alkali
604 aluminosilicate melts. Geochimica et Cosmochimica Acta, 65(14), 2413-2431.
605 Mysen, B.O., and Cody, G.D. (2004) Solubility and solution mechanism of H_2O in alkali
606 silicate melts and glasses at high pressure and temperature. Geochimica et
607 cosmochimica Acta, 68(24), 5113-5126.
608 Mysen, B.O., and Cody, G.D. (2005) Solution mechanisms of H_2O in depolymerized
609 peralkaline melts. Geochimica et Cosmochimica Acta, 69(23), 5557-5566.
610 Mysen, B.O., and Richet, P. (2005) Silicate Glasses and Melts, Properties and Structure.
611 Elsevier, Amsterdam.
612 Mysen, B.O., Finger, L.W., Virgo, D., and Seifert, F.A. (1982) Curve-fitting of Raman
613 spectra of silicate glasses. American Mineralogist, 67(7-8), 686-695.
614 Mysen, B.O., Lucier, A., and Cody, G.D. (2003) The structural behavior of Al^{3+} in
615 peralkaline melts and glasses in the system $Na_2O-Al_2O_3-SiO_2$. American
616 Mineralogist, 88, 1668-1678.
617 Mysen, B.O., Cody, G.D., and Smith, A. (2004) Solubility mechanisms of fluorine in
618 peralkaline and meta-aluminous silicate glasses and in melts to magmatic

temperatures. Geochimica et Cosmochimica Acta, 68(12), 2745–2769.

Osborn E.F, and Muan A. (1960) Phase equilibrium diagrams for ceramists. Plate 4. The system Na_2O-Al_2O_3-SiO_2. American Ceramic Society, Columbus, OH.

Sandland, T.O., Du, L.S., Stebbins, J.F., and Webster, J.D. (2004) Structure of Cl-containing silicate and aluminosilicate glasses: A ^{35}Cl MAS-NMR study. Geochimica et cosmochimica acta, 68(24), 5059-5069.

Schaller, T., and Sebald, A. (1995) One- and two-dimensional ^{1}H magic- angle spinning experiments on hydrous silicate glasses. Solid State Nuclear Magnetic Resonance 5, 89-102.

Schaller, T., Dingwell, D.B., Keppler, H., Knöller, W., Merwin, L., and Sebald, A. (1992) Fluorine in silicate glasses: A multinuclear nuclear magnetic resonance study. Geochimica et Cosmochimica Acta, 56, 701–707.

Stebbins, J.F., and Du, L.-S. (2002) Chloride ion sites in silicate and aluminosilicate glasses: A preliminary study by ^{35}Cl solid-state NMR. American Mineralogist, 87, 359-363.

Webster, J.D. (1997) Chloride solubility in felsic melts and the role of chloride in magmatic degassing. Journal of Petrology, 38, 1793-1807.

Xue, X., and Kanzaki, M. (2003) The dissolution mechanism of water in alkaline earth silicate and aluminosilicate melts: one view from ^{1}H MAS NMR. Geochimica et Cosmochimica Acta, 67, A543.

Yamamoto K., Nakanishi T., Kasahara H., and Abe K. (1983) Raman scattering of SiF_4 molecules in amorphous fluorinated silicon. Journal of Non-Crystalline Solids, 59-60, 213-216.

Zeng, Q., and Stebbins, J.F. (2000) Fluoride sites in aluminosilicate glasses: High-resolution ^{19}F NMR results. American Mineralogist, 85, 863-867.

Zhang Y., and Stolper, E. M. (1991) Water diffusion in a basaltic melt. Nature 351, 306-309.

Zimova, M., and Webb, S.L. (2006) The effect of chlorine on the viscosity of Na_2O-Fe_2O_3-Al_2O_3-SiO_2 melts. American Mineralogist, 91(2-3), 344–352.

Zotov, N., and Keppler, H. (1998) The influence of water on the structure of hydrous sodium tetrasilicate glasses. American Mineralogist, 83, 823-834.

FIGURE CAPTIONS

664 **Figure 1.** Solubility (mol%) of F (A) and Cl (B) in aluminosilicate quenched melts
665 (glass) as a function of the H_2O content in wt%. For F-solubility experiments, diamonds
666 refer to NS5Ax samples and, for Cl-solubility experiments, circles refer to NS3Ax
667 samples. The gray scale refers to the bulk Al_2O_3 content (mol%). All samples were run at
668 1.5 GPa and 1400ºC. Errors bars in F and Cl mol% represent one standard deviation of
669 the average of all analyses of each sample (≥ 12 analyses). Error bars in H_2O content
670 (1.08 wt%) represent the analytical error, calculated from the difference between known
671 standards' composition values and their measured values (see text for standards
672 description).
673
674 **Figure 2.** Illustration of background subtraction with the Raman spectrum of glass
675 C5H2NS4 as an example.
676
677 **Figure 3.** Raman spectra of NS4Ax glasses in the frequency region of first-order Raman
678 scattering, for composition indicated in individuals panels. Numbers on individual spectra
679 denotes the measured H_2O content (wt%). Spectra are offset for clarity and are
680 normalized to 100% intensity, where 100% represents that data point within each
681 spectrum of the highest intensity.
682
683 **Figure 4.** Examples of Raman spectra of glasses in the frequency region on (Si, Al)-O
684 stretch vibrations for compositions indicated on each figure. The individual lines are of
685 Gaussian shape and fitted to the spectra as discussed in the text. Also see text for
686 discussion of band assignments.

687

688 **Figure 5.** Mol fraction of Q^1, X_{Q1}, Q^2, X_{Q2}, Q^3, X_{Q3}, and Q^4, X_{Q4}, structural units as a
689 function of H_2O content (wt%), in halogen-free samples (squares), in F-bearing samples
690 (diamonds) and in Cl-bearing samples (circles), in the system NS4. Data in the halogen-
691 free samples are from Mysen (2007). Q^n species abundance was calculated from Raman
692 data by using equation 1 and 2 and calibration factors from Mysen and Cody (2005),
693 except for Q^4, which was calculated by mass balance following equation 2. For more
694 clarity, only errors on X_{Qn} abundances, calculated from the fitting procedure, are
695 reported. Errors on H_2O content for those samples are presented in Figure 2.

696

697 **Figure 6.** Mol fraction of Q^1, X_{Q1}, Q^2, X_{Q2}, Q^3, X_{Q3}, and Q^4, X_{Q4}, structural units as a
698 function of H_2O content (wt%), in halogen-free samples (squares), in F-bearing samples
699 (diamonds) and in Cl-bearing samples (circles), in the system NS4A10. Data in the
700 halogen-free samples are from Mysen (2007).

701

702 **Figure 7.** Degree of polymerization, NBO/T (T = Si + Al), of the glasses in NS4 system
703 (A) and in the NS4A10 system (B), as a function of mol% H_2O. Symbols are the same as
704 that used in Figures 5 and 6.

705

706

707

TABLE 1. Composition of starting glasses (wt%)

	NS3A0 [13]	NS3A5 [12]	NS3A10 [12]
SiO_2	75.96(57)	64.98(62)	52.41(31)
Al_2O_3	—-	7.84(10)	15.86(19)
Na_2O	23.75(70)	28.06(28)	32.09(37)
Total	99.71	100.89	100.36
Al/(Al+Si)[b]	0	0.12	0.26
NBO/T	0.61	0.61	0.61
	NS5A0 [12]	NS5A5 [12]	NS5A10 [13]
SiO_2	83.84(41)	70.17(79)	59.49(68)
Al_2O_3	—-	9.14(20)	15.54(81)
Na_2O	16.34(16)	21.51(60)	24.84(72)
Total	100.18	100.81	99.87
Al/(Al+Si)	0	0.13	0.24
NBO/T	0.38	0.38	0.38
	NS4A0 [12]	NS4A5 [12]	NS4A10 [11]
SiO_2	79.65(55)	68.16(43)	54.03(38)
Al_2O_3	—-	7.96(14)	17.21(32)
Na_2O	19.74(21)	24(51(19)	29.37(29)
Total	99.4	100.62	100.62
Al/(Al+Si)	0	0.12	0.27
NBO/T	0.48	0.49	0.49

Notes: Numbers in brackets indicate number of individual electron microscope analyses included on average. Number in parentheses represents one standard deviation in terms of the least units cited.

[a] Calculated from composition assuming that Si^{4+} and Al^{3+} are in tetrahedral coordination in the glasses.

TABLE 2. Composition of run products **{{center Solubility samples over H2O and F mol% and put straddle rule}}**

Sample	Solubility samples H_2O wt%	F mol%	Cl mol%
	NBO/T[b] = 0.38(1)		
Al/(Al +Si) [a] = 0			
F10NS5	0	3.33(73)	—
F10H2NS5	2.01	3.51(46)	—
F10H4NS5	7.34	3.84(62)	—
F10H8NS5	9.01	4.41(3)	—
F10H10NS5	9.50	4.98(6)	—

Al/(Al +Si) = 0.12			
F10NS5A5	0	4.29(36)	—
F10H4NS5A5	7.67	4.95(41)	—
F10H6NS5A5	8.72	5.57(8)	—
F10H8NS5A5	8.78	6.14(41)	—
Al/(Al +Si) = 0.24			
F10NS5A10	0	6.31(37)	—
F10H2NS5A10	3.08	6.97(50)	—
F10H4NS5A10	3.31	7.32(92)	—
F10H6NS5A10	5.41	7.53(80)	—
F10H8NS5A10	10.64	9.37(93)	—
F10H10NS5A10	10.69	9.91(30)	—
	NBO/T = 0.61(1)		
Al/(Al +Si) = 0			
C5NS3	0	—	5.70(65)
C5H2NS3	1.90	—	5.1(12)
C5H4NS3	3.04	—	4.79(11)
C5H6NS3	7.18	—	4.07(10)
C5H8NS3	7.57	—	3.58(8)
C5H10NS3	8.95	—	3.4(6)
Al/(Al +Si) = 0.13			
C5NS3A5	0	—	3.94(66)
C5H2NS3A5	2.51	—	3.62(10)
C5H4NS3A5	3.62	—	3.39(10)
C5H8NS3A5	4.43	—	2.91(8)
C5H10NS3A5	4.87	—	2.64(7)
Al/(Al +Si) = 0.26			
C5NS3A10	0	—	3.86(38)
C5H2NS3A10	2.80	—	2.15(6)
C5H4NS3A10	5.42	—	2.04(6)
C5H6NS3A10	6.84	—	1.93(5)
C5H8NS3A10	7.78	—	1.81(5)
C5H10NS3A10	8.53	—	1.66(4)

Notes: Numbers in parentheses represents one standard deviation in terms of least units cited. Dash = below the detection limit.

[a] Calculated from composition assuming that Si^{4+} and Al^{3+} are in tetrahedral coordination in the glasses.

[b] NBO/T from composition of starting glasses.

TABLE 3. Parameters of the best curve-fits of Raman spectra: peak location (cm^{-1}), full-width at half maximum (FWHM, cm^{-1}) and not normalized peak areas

	Peak location						Peak FWHM								
	Q^1	Q^2	Si-F	Si-O^o	Q^3	Q^4	Q^1	Q^2	Si-F	Si-O^o	Q^3	Q^4	$Q^1(\sigma)$	$Q^2(\sigma)$	Si-F(σ)
F10NS4*	—	953	995	1035	1092	1148	–	54	38	45	69	81	—	50400(201)	51015(198)
F10H2NS4	889	969	1002	1045	1085	1147	65	72	56	52	61	70	5277(125)	19902(125)	17160(155)
F10H6NS4	890	946	997	1024	1066	1136	54	57	55	49	67	78	12941(87)	18737(118)	43135(279)
F10H10NS4	892	944	994	1002	1050	1132	57	57	57	42	69	81	25204(141)	31151(139)	79747(227)
F10NS4A10*	—	939	999	1050	1094	1153	–	74	81	65	70	74	—	100250(357)	248954(446)
F10H2NS4A10	878	944	988	1030	1057	1110	69	64	51	63	60	66	26342(360)	69601(399)	100945(538)
F10H6NS4A10	889	944	993	1025	1056	1101	61	62	49	50	55	66	15860(354)	66841(327)	64764(520)
F10H10NS410	866	936	980	1015	1052	1097	69	60	55	51	56	65	39201(96)	71148(129)	73668(330)
C5NS4*	—	958	—	1029	1087	1140	—	64	—	72	57	88	—	41854(637)	—
C5H2NS4	906	966	—	1024	1075	1133	55	54	—	71	58	79	9282(108)	23139(323)	—
C5H6NS4	895	957	—	1005	1059	1130	59	63	—	60	62	83	11305(141)	24923(165)	—
C5H10NS4	903	964	—	1009	1060	1133	54	57	—	57	58	85	10737(73)	26944(171)	—
C5NS4A10*	—	945	—	1005	1073	1128	—	70	—	81	78	86	—	67133(354))	—
C5H2NS4A10	878	952	—	1007	1058	1110	64	70	—	72	66	78	12964(72)	38552(97)	—
C5H6NS4A10	878	957	—	1004	1052	1102	62	73	—	53	58	80	11872(95)	47869(215)	—
C5H10NS410	875	958	—	1004	1054	1111	65	73	—	56	58	83	16333(39)	33315(108)	—

Notes: Number in parentheses represents one standard deviation in terms of the least units cited. Dash = not determined.
* from Dalou et al. (in review).

TABLE 4. Volatiles and silicate species abundance from Raman spectra of F and Cl-bearing NS4 and NS4A10 glasses

	H_2O	F	Cl	SiF %	Relative peak area				Rel
	wt%[a]	Mol%	Mol%	[b]	Q^1	Q^2	Q^3	Q^4	Q^1
F10NS4*	n.a.	3.95(2)	–	0.06(1)	—	0.07(0.2)	0.65(4)	0.28(1)	—
F10H2NS4	3.86	2.92(50)	–	0.04(1)	0.02(0.04)	0.06(0.05)	0.64(0.08)	0.28(0.07)	0.004(0.2)
F10H6NS4	6.65	4.00(39)	–	0.15(4)	0.06 (0.04)	0.08(0.05)	0.64(0.1)	0.22(0.08)	0.01(0.3)
F10H10NS4	11.14	3.46(63)	–	0.22(4)	0.11(0.06)	0.13(0.06)	0.59 (0.09)	0.17(0.06)	0.02(0.6)

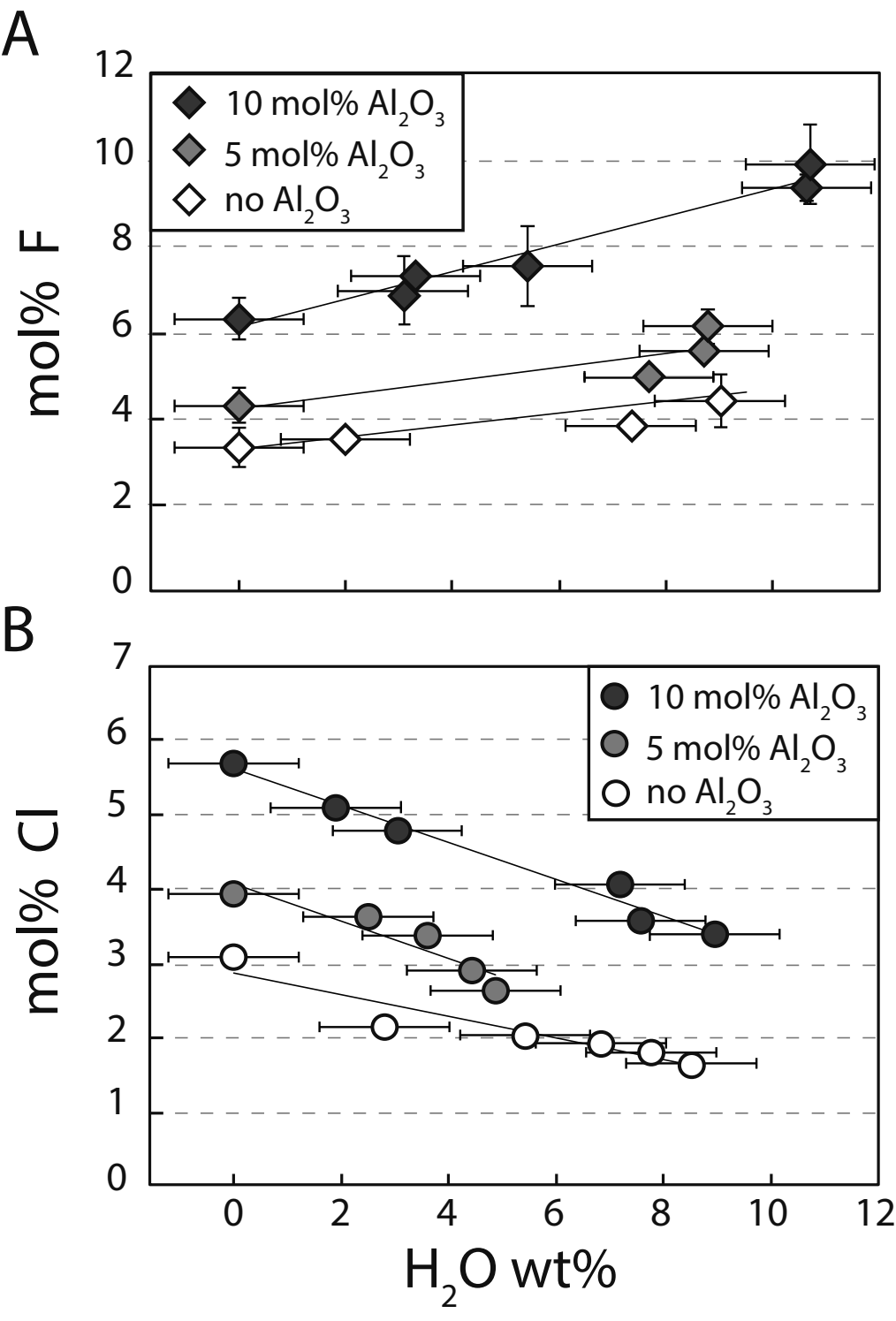
A
B
10 mol% Al2O3
5 mol% Al2O3
no Al2O3
mol% F
mol% Cl
H2O wt%
0
2
4
6
8
10
12

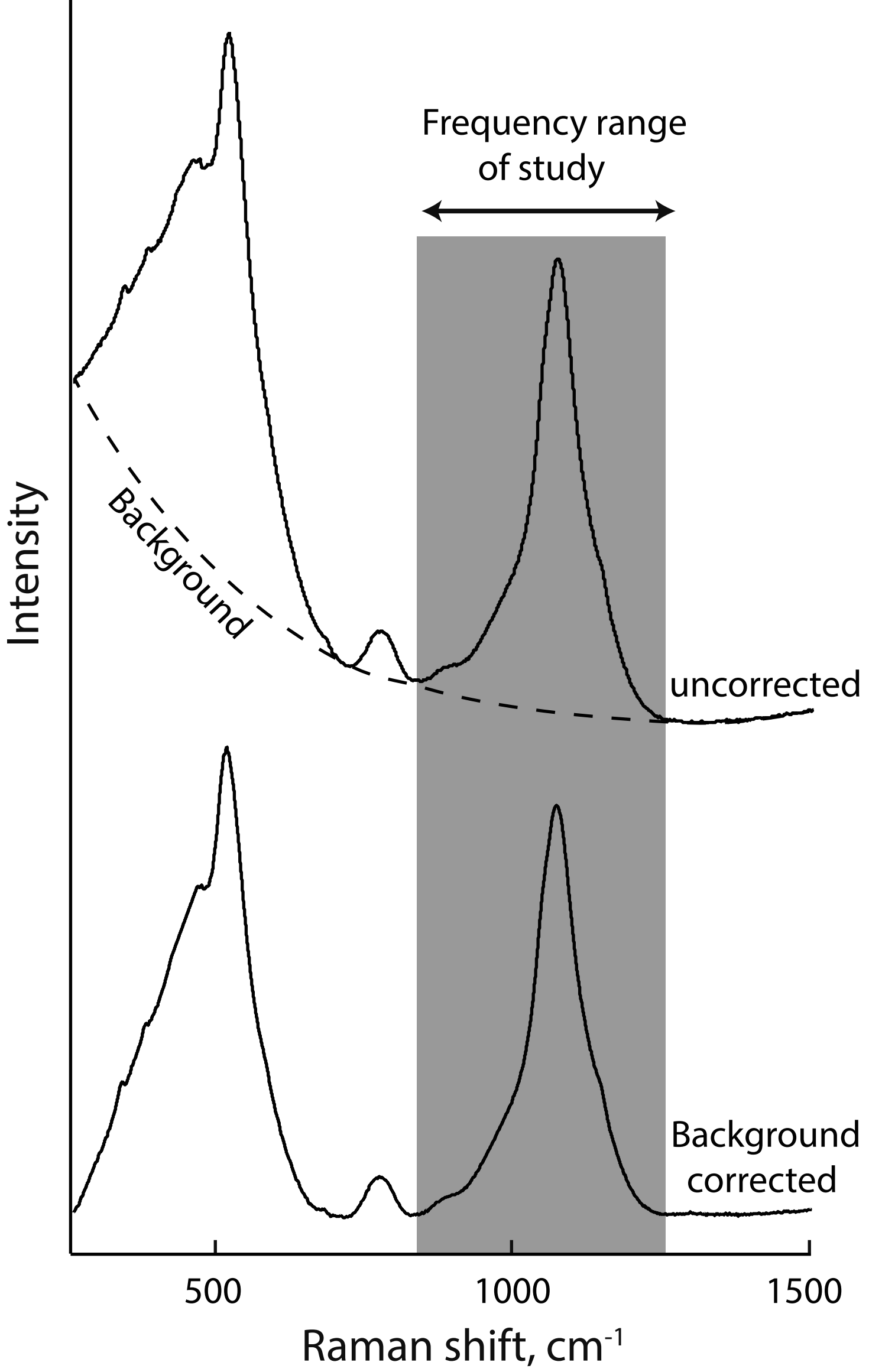
Frequency range
of study
Background
uncorrected
Background
corrected
Intensity
500
1000
1500
Raman shift, cm-1

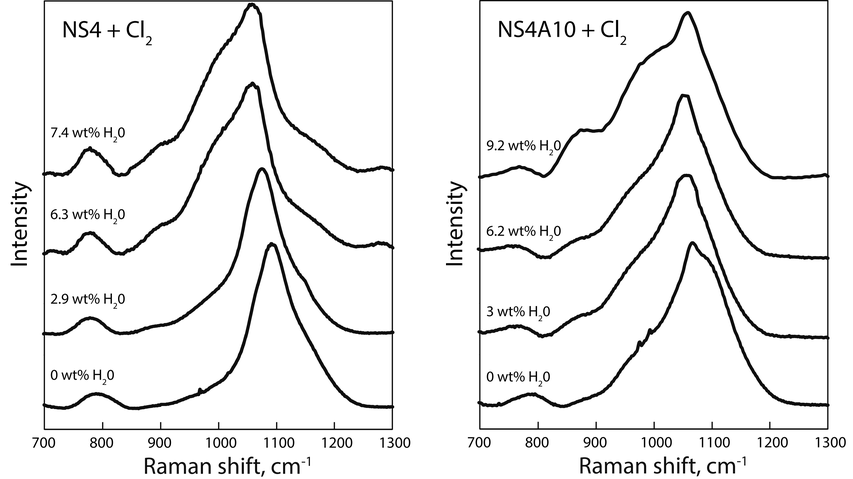
NS4 + Cl2
7.4 wt% H20
6.3 wt% H20
2.9 wt% H20
0 wt% H20
Intensity
700 800 900 1000 1100 1200 1300
Raman shift, cm-1

NS4A10 + Cl2
9.2 wt% H20
6.2 wt% H20
3 wt% H20
0 wt% H20
Intensity
700 800 900 1000 1100 1200 1300
Raman shift, cm-1

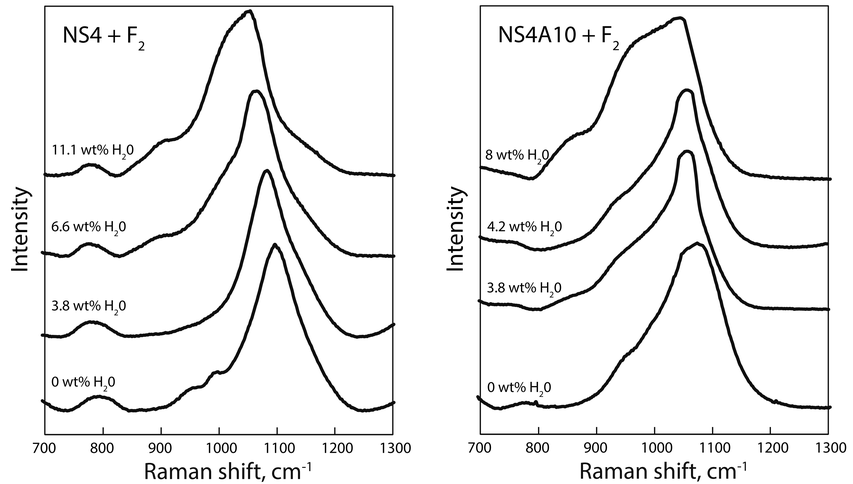
NS4 + F2
11.1 wt% H20
6.6 wt% H20
3.8 wt% H20
0 wt% H20
Intensity
700 800 900 1000 1100 1200 1300
Raman shift, cm-1

NS4A10 + F2
8 wt% H20
4.2 wt% H20
3.8 wt% H20
0 wt% H20
Intensity
700 800 900 1000 1100 1200 1300
Raman shift, cm-1

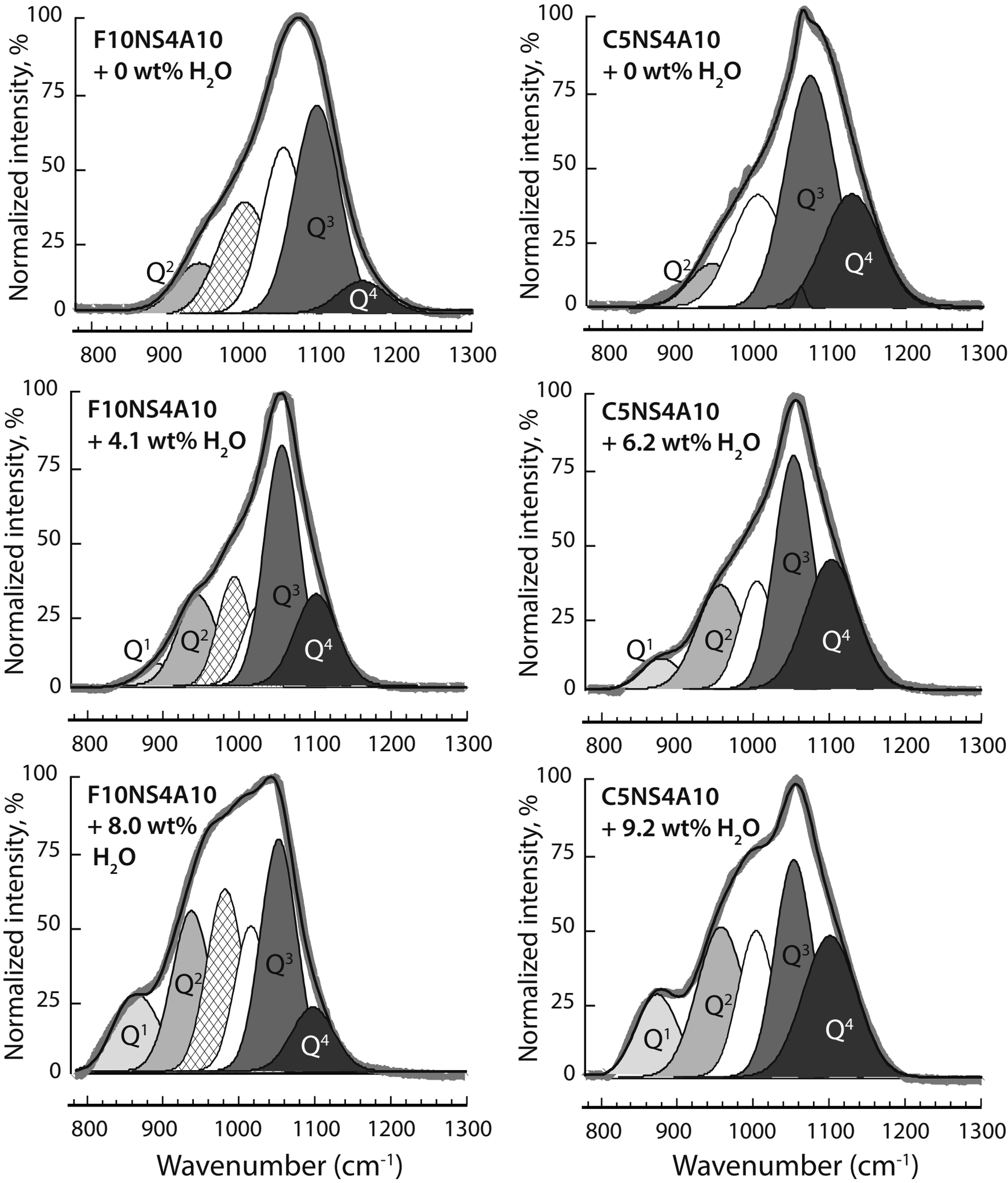
F10NS4A10
+ 0 wt% H2O
C5NS4A10
+ 0 wt% H2O
F10NS4A10
+ 4.1 wt% H2O
C5NS4A10
+ 6.2 wt% H2O
F10NS4A10
+ 8.0 wt%
H2O
C5NS4A10
+ 9.2 wt% H2O
Normalized intensity, %
Wavenumber (cm-1)
Q1
Q2
Q3
Q4
0
25
50
75
100
800
900
1000
1100
1200
1300

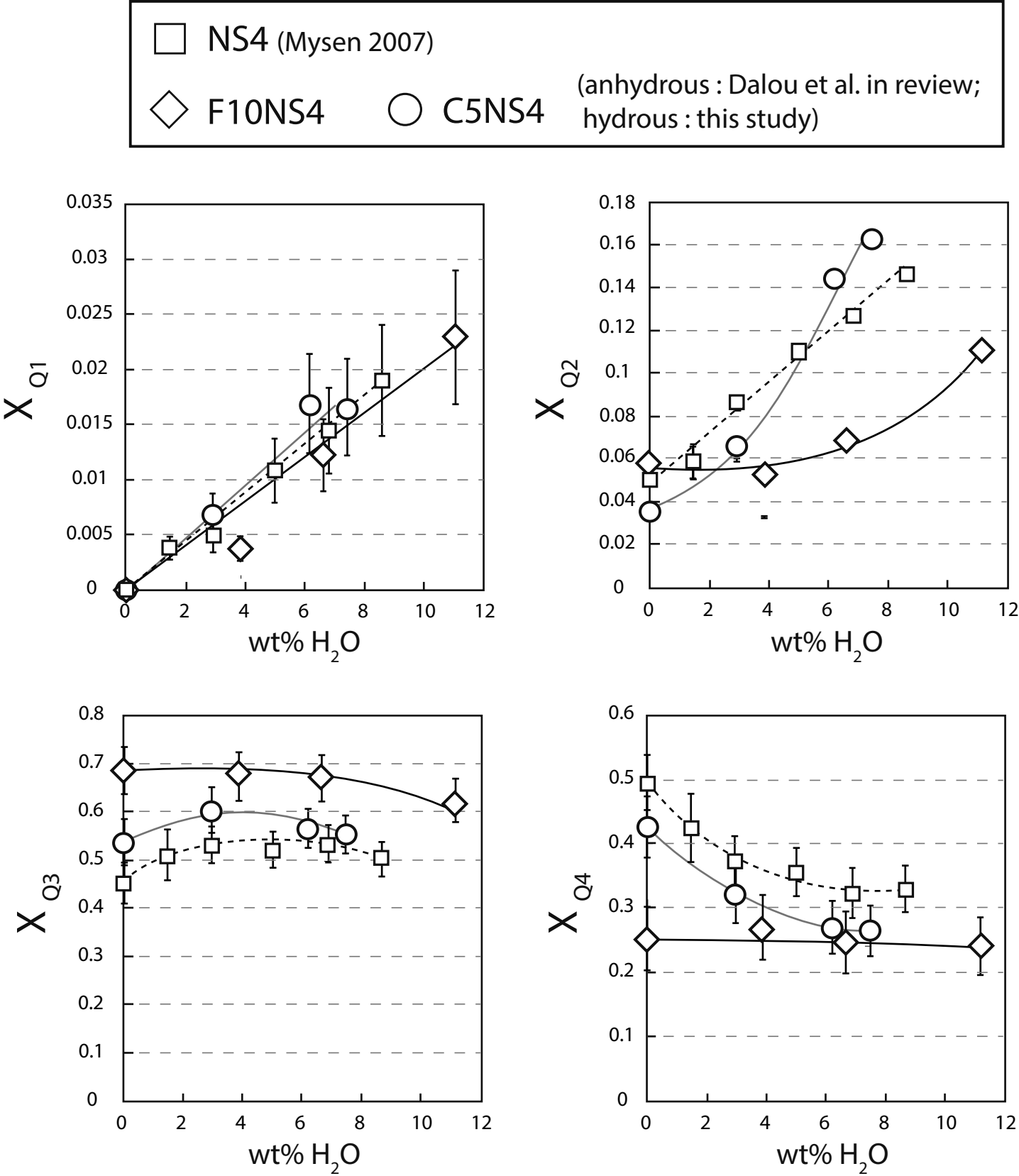
NS4 (Mysen 2007)
F10NS4
C5NS4
(anhydrous : Dalou et al. in review;
hydrous : this study)
X Q1
X Q2
X Q3
X Q4
wt% H2O
wt% H2O
wt% H2O
wt% H2O

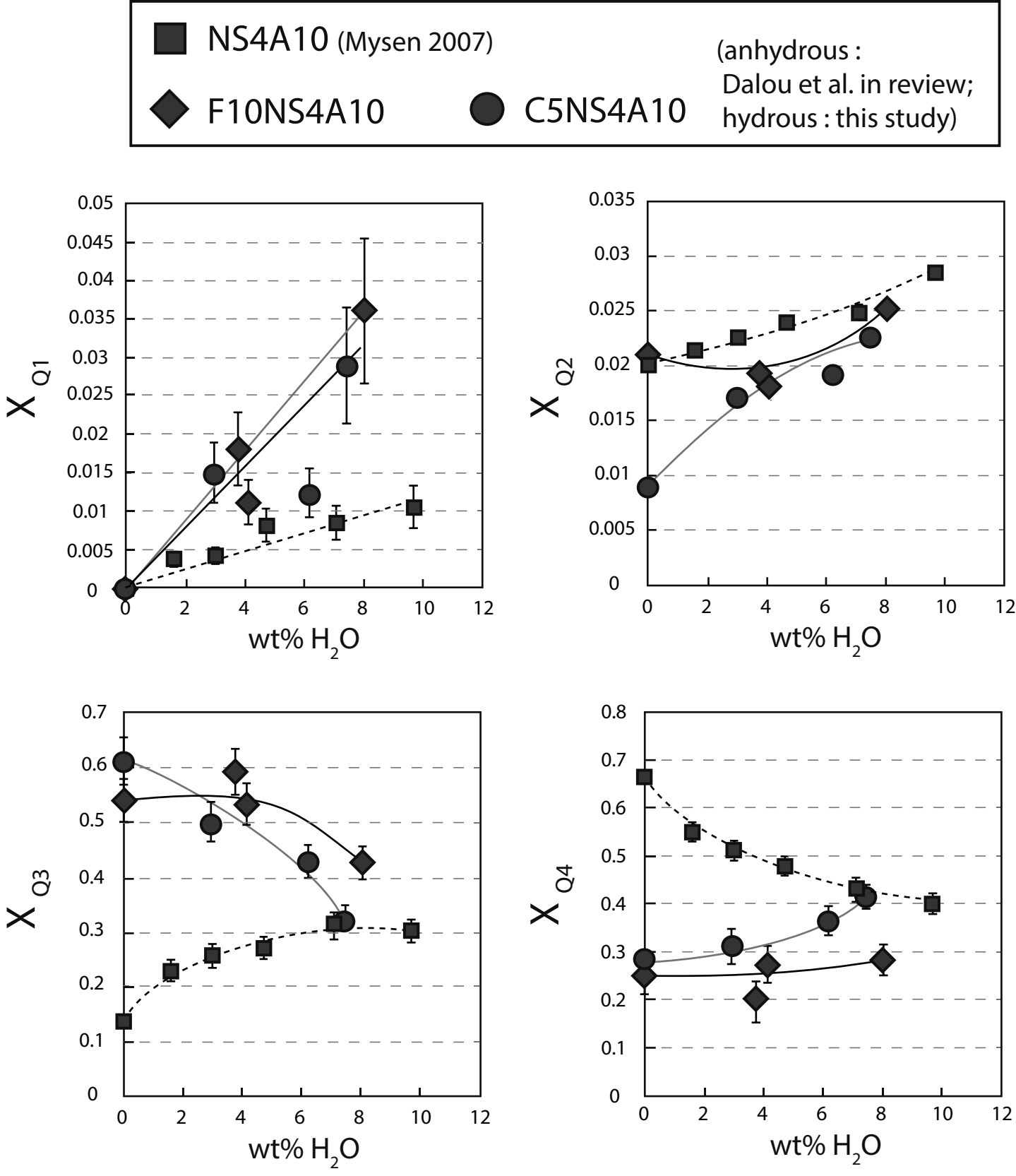
NS4A10 (Mysen 2007)
F10NS4A10
C5NS4A10
(anhydrous :
Dalou et al. in review;
hydrous : this study)
X Q1
X Q2
X Q3
X Q4
wt% H2O
wt% H2O
wt% H2O
wt% H2O

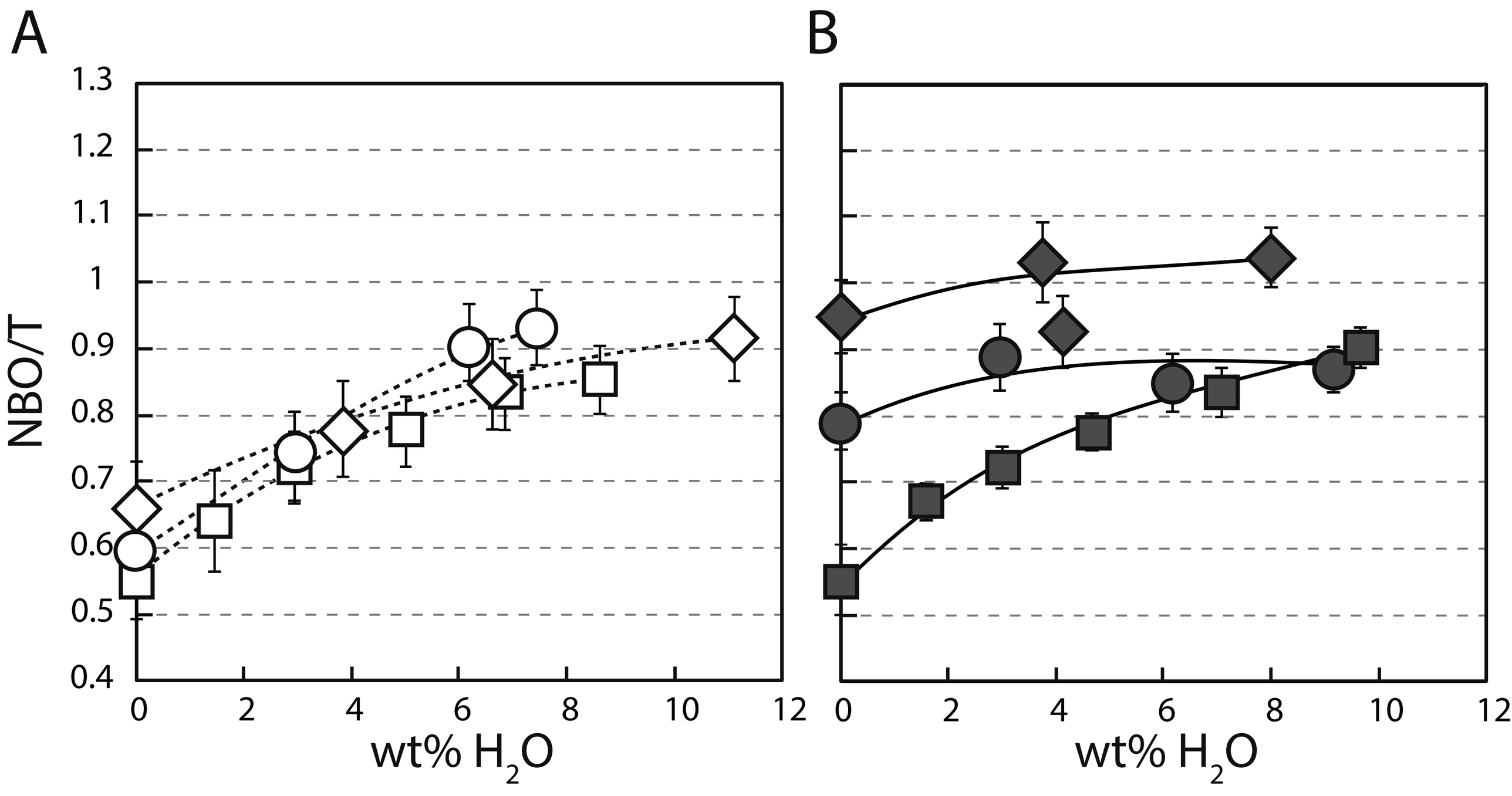
A
B
NBO/T
1.3
1.2
1.1
1
0.9
0.8
0.7
0.6
0.5
0.4
0
2
4
6
8
10
12
wt% H2O
wt% H2O